第38卷第3期 2022年3月
无 机 化 学 学 报 CHINESE JOURNAL OF INORGANIC CHEMISTRY
Vol.38 No.3 559-568

基于1,4,5,8-萘四羧酸原位合成的钡配合物的结构、对芳香胺的检测及其作为纳米$BaCO_3$的前驱体

黄小冬[1] 程炯佳[2] 陶程龙[2] 王 健[2] 王小锋*[,2] 吴 刚[3] 刘光祥[2]
([1]南京师范大学化学与材料科学学院,南京 210023)
([2]南京晓庄学院环境科学学院,南京 211171)
([3]滁州学院材料与化学工程学院,滁州 239012)

摘要: 以1,4,5,8-萘四羧酸为原料,在溶剂热条件下原位反应合成得到一个具有3D拓扑结构的发光钡基金属有机骨架(MOF):$[Ba(dna)(H_2O)_2]_n$(**1**,H_2dna=1,8-萘二甲酸酐-4,5-二羧酸),并通过单晶X射线衍射、元素分析、热重分析和粉末X射线衍射技术对其进行表征。结构分析表明,**1**包含一个π共轭基团和酸酐基团的有机配体dna^{2-},荧光和紫外研究表明其能灵敏地检测溶液中的芳香胺,可能是MOF结构中配体的酸酐基团和氨基之间的反应驱动的,这大大提高了荧光发射强度,并达到裸眼可见的颜色变化。此外,以配合物**1**为前驱体在中等温度下直接煅烧制得了单一晶型的纳米$BaCO_3$颗粒。

关键词: Ba(Ⅱ)配合物; 羧基; 荧光性质; $BaCO_3$粒子
中图分类号: O614.23+3 **文献标识码:** A **文章编号:** 1001-4861(2022)03-0559-10
DOI: 10.11862/CJIC.2022.053

Barium Complex *In Situ* Synthesized from 1,4,5,8-Naphthalene Tetracarboxylic Acid: Structure, Detection of Aromatic Amines, and Use as a Precursor of Nano $BaCO_3$

HUANG Xiao-Dong[1] CHENG Jiong-Jia[2] TAO Cheng-Long[2]
WANG Jian[2] WANG Xiao-Feng*[,2] WU Gang[3] LIU Guang-Xiang[2]
([1]*School of Chemistry and Materials Science, Nanjing Normal University, Nanjing* 210023, *China*)
([2]*College of Environmental Science, Nanjing Xiaozhuang University, Nanjing* 211171, *China*)
([3]*College of Material and Chemical Engineering, Chuzhou University, Chuzhou, Anhui* 239012, *China*)

Abstract: Using 1,4,5,8-naphthalene tetracarboxylic acid as a raw material, a luminescent barium-based metal-organic framework (MOF), $[Ba(dna)(H_2O)_2]_n$ (**1**, H_2dna=1,8-naphthalic anhydride-4,5-dicarboxylic), with a 3D topological structure was synthesized by *in situ* reaction under solvothermal conditions, and characterized by single-crystal X-ray diffraction, elemental analysis, thermogravimetric analysis, and powder X-ray diffraction. The structural analysis demonstrates that it has the underlying 3D topology, encompassing a π-conjugated organic ligand with an anhydride group. It exhibited a low detection limit for aromatic amines in an aqueous solution, which may be driven by an anhydride amine reaction between the ligand and the hosted amines, with a significant enhancement of the emission intensity and visual color change. Furthermore, micro-crystalline $BaCO_3$ particles can be prepared through direct calcination of complex **1** as a precursor at moderately elevated temperatures. CCDC: 2026609.

Keywords: Ba(Ⅱ) complex; carboxylate group; luminescent property; $BaCO_3$ particles

收稿日期:2021-09-24。收修改稿日期:2021-12-27。
国家自然科学基金(No.21671107)、江苏省大学生创新创业训练项目(No.202011460070Y)、南京晓庄学院2017年度校级重点项目(No.2017NXY11)、南京晓庄学院校级大创项目(No.2020XSKY089)和滁州学院科研启动项目(No.2014qd035)资助。
*通信联系人。E-mail:wangxf0215@163.com,Telephone:+86-25-86178274,Fax:+86-25-86178274

0 Introduction

Detecting poisonous chemicals at a very low limit is crucial because leakage or loss of control of those can lead to widespread risks to the environment, even at very low concentrations[1-3]. Evaluating the poisonous amines, one kind of the most hazardous and wide-spreading chemicals, is of great importance for pollution control. Additionally, there is another instant requirement for detection of amines in our daily life, like control of food quality, and management of some diseases[4-6]. Various techniques have been developed and applied to detect poisonous amines, including classic gas and liquid chromatography, mass spectrometry, light-emitting sensing, and electrochemical sensing methods. Particularly, light-emitting sensing methods are gaining more attention attributed to their practical sensitivity, simple handling procedures, and rapid response time. Accordingly, most of the sensing methods are based on fluorescence changes due to the high selectivity and sensitivity of fluorescence sensing[7-8]. Fluorescence quenching is the most common one in those sensing principles of probes, while probes of "turn-on" fluorescence enhancement for sensing of amines are more applicable than those of fluorescence quenching[9-11]. Therefore, it is still attractive to construct a sensor with a "turn-on" property.

Recently, metal-organic frameworks (MOFs) have been well-established as sensors owing to their fast, reversible, and recyclable sensing capacity[12-17]. MOFs materials are superior to other porous materials because of their high/tunable porosity, pore functionality, various pore architectures/compositions, open metal sites, which control the molecular level interaction and selectivity between the framework and probe analytes[18-20]. There are full of challenges to designing and synthesizing MOFs for distinguishable "turn-on" recognition of amines through interactions between ligand and amines, which can regulate the MOF photoluminescence (PL). Polycarboxylate ligands are good building blocks for the construction of luminescent MOFs networks because they can adopt a variety of coordination modes such as monodentate, chelating-bidentate, bridging-bidentate, and bridging-multidentate patterns[21-23]. Meanwhile, compared with transition metal ions, alkaline earth metals generally have high and variable coordination numbers and can provide a flexible coordination environment because of their large ion radius, leading to a large number of MOFs with diverse structures[24-27].

Herein, we successfully synthesized a luminescent barium metal-organic framework $[Ba(dna)(H_2O)_2]_n$ (**1**) using a π-conjugated, electron-deficient, carboxyl-functionalized ligand 1,4,5,8-naphthalene tetracarboxylic acid (nta), which was further converted to 1,8-naphthalic anhydride-4,5-dicarboxylic (H_2dna) after the solvothermal reaction with $BaCO_3$. This novel Ba-MOF complex with high chemical stability can afford as a "turn-on" sensing probe for aromatic amines at a low detection limit. Based on direct calcination of complex **1**, a simple method was further developed to produce micro-crystalline $BaCO_3$ particles.

1 Experimental

1.1 Materials and methods

1,4,5,8-Naphthalene tetracarboxylic acid (98%), $BaCO_3$, phenylamine, naphthylamine, and 1-aminopyrene were purchased from J&K. Other reagents such as methanol and ethanol were purchased from Sinopharm Chemical Reagent Co., Ltd. All commercially available agents were of reagent grade and used as received without further purification. C and H analyses were made on a Perkin-Elmer 240C elemental analyzer. IR spectrum was recorded on Nicolet 6700 FT-IR spectrophotometer by using KBr pellet in a range of 4 000-400 cm^{-1}. Thermogravimetric analysis (TGA) was performed with a simultaneous SDT Q600 thermal analyzer under 100.0 $mL\cdot min^{-1}$ flowing nitrogen with a heating rate of 20 $℃\cdot min^{-1}$ from room temperature to 800 ℃. The luminescent spectra for the samples were recorded at room temperature on CaryEclipse 300 spectrophotometer with a xenon arc lamp as the light source. In the measurements of the emission and excitation spectra, the pass width was 5.0 nm. Powder X-ray diffraction (PXRD) patterns were performed with a Bruker D8 ADVANCE X-ray diffractometer with Cu $K\alpha$ radiation (λ=0.154 06 nm, U=45 kV, I=40 mA, 2θ=10°-70°).

The micro morphology of the synthesized material were observed by a JEOL JSM 5600LV at 20 kV.

1.2 Synthesis of $[Ba(dna)(H_2O)_2]_n$ (1)

The mixture of nta (15.2 mg, 0.05 mmol) and $BaCO_3$ (7.9 mg, 0.04 mmol) in 4 mL distilled water and 12 mL ethanol was heated for about 20 h in a 25 mL Teflon-lined stainless-steel container at 160 ℃. The mixture was cooled to room temperature, and brown crystal **1** (5.6 mg, 48% yield based on Ba) were obtained by filtration and dried in air. Elements analyses Calcd. for $C_{14}H_8BaO_9$(%): C, 36.75; H, 1.76. Found: C, 36.72; H, 1.78. FT-IR spectrum (cm^{-1}): 3 405(bs), 1 776(s), 1 706(s), 1 605(s), 1 590(s), 1 440(m), 1 398(m), 1 383(m), 1 337(m), 1 226(w), 1 190(w), 1 160(w), 1 128(w), 1 051(m), 1 016(w), 872(m), 828(m), 778(m), 745(w), 596(w).

1.3 X-ray crystallography

Data collection for complex **1** (0.33 mm×0.28 mm×0.25 mm) was performed on a Bruker Smart APEX Ⅱ CCD diffractometer at 296 K by using a graphite-monothematic Mo $K\alpha$ radiation (λ=0.071 073 nm). A total of 9 136 reflections were collected, of which 3 049 (R_{int}=0.018 4) were independent in a θ range of 2.86°-27.53°. The absorption corrections were applied using the SADABS program. Structural solutions were performed by direct methods using the SHELXS-97 program and the structures were refined by full-matrix least-squares techniques with SHELXL-97. All non-hydrogen atoms were placed in successive difference Fourier syntheses and refined with anisotropic thermal parameters on F^2. The hydrogen atoms were geometrically generated and refined by a riding mode. The hydrogen atoms were generated geometrically.

CCDC: 2026609.

1.4 UV-Vis spectra, luminescence spectra, and detection of aromatic amines

First, the luminescence emission spectra of **1** and ligand nta on solid states were recorded at room temperature. To determine the absorbance of aromatic amines, the UV-Vis spectra of all the samples were measured in water solution and ultrasonically dispersed before the test. Complex **1** was prepared into 1 mg·mL^{-1} water solution in a homogeneous dispersion state using ultrasonic. The tested samples with aromatic amines were got first from the reaction of 1 mL above **1** solution (Calcd. 1 mg) with given amounts of the aqueous solution of amines (all in 0.1 mg·mL^{-1}) added, and reacted at 50 ℃ for 15 min. Then the solid was centrifuged and washed three times with 5 mL ethanol and 5 mL water separately, finally diluted and dispersed to 1 mL water solution. The samples for UV-Vis test and luminescence test in solution state were transferred 100 μL from as-prepared above solutions and diluted to 2 mL for the test.

2 Results and discussion

2.1 Crystal structure of complex 1

Single-crystal X-ray structure analysis reveals that complex **1** crystallizes in the triclinic $P\bar{1}$ space group and the detailed crystallographic data are exhibited in Table 1. As shown in Fig.1, the asymmetric unit of **1** consists of one unique Ba(Ⅱ) ion, one unique dna^{2-} ligand, and two coordinated water molecules. The Ba(Ⅱ) ion has a nine-coordinate configuration, consisting of

Table 1 Crystallographic data of complex 1

Parameter	1
Chemical formula	$C_{14}H_8BaO_9$
Formula weight	457.54
crystal system	Triclinic
Space group	$P\bar{1}$
a / nm	0.717 05(6)
b /nm	0.828 50(7)
c / nm	1.160 65(10)
α / (°)	75.836(2)
β / (°)	84.036(2)
γ / (°)	87.866(2)
V / nm^3	0.664 88(10)
Z	2
D_c / (g·cm^{-3})	2.285
μ (Mo $K\alpha$) / mm^{-1}	3.041
Unique reflection	3 049
Observed reflection	2 918
R_{int}	0.018 4
F(000)	440
R_1, wR_2 (all data)	0.019 1, 0.051 2
R_1, wR_2 [$I>2\sigma(I)$][a,b]	0.017 9, 0.050 4
GOF	1.002

[a] $R_1=\sum||F_o|-|F_c||/\sum|F_o|$; [b] $wR_2=\{\sum[w(|F_o|^2-|F_c|^2)^2]/\sum[w(|F_o|^2)^2]\}^{1/2}$.

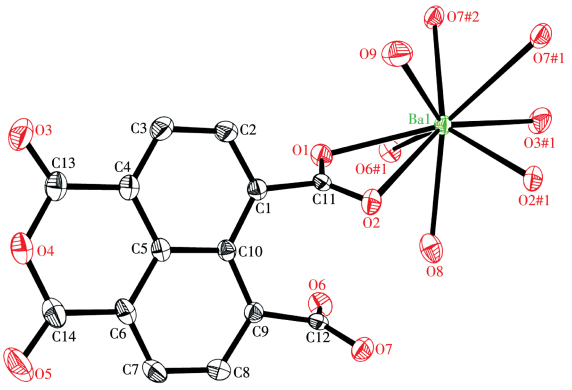

Hydrogen atoms are omitted for clarity; Symmetry codes: #1: 1−*x*, −*y*, 1−*z*; #2: 1−*x*, −1−*y*, 1−*z*

Fig.1 Coordination geometry of complex **1** drawn at 30% probability displacement ellipsoids

seven carboxylate oxygen atoms from six different dna^{2-} ligands and two oxygen donors from two coordinated water molecules, which form a distorted mono-capped square geometry architecture. As listed in Table 2, the Ba—O distances range from 0.261 98(17) to 0.323 07(18) nm, which are similar to those observed in the reported complexes[24-25]. The O—Ba—O bond angles fall in a range of 42.27(5)°-153.93(6)°.

In **1**, ligand nta was deprotonated completely and converted to dna^{2-} as a μ_5-bridge linking five Ba(Ⅱ) ions, in which two carboxylate groups adopt two μ_3-η^1:η^2 and μ_2-η^2:η^1 coordination fashions, respectively (Scheme 1). The dihedral angle between the center naphthalene ring and anhydride group (O3, C13, O4, C14, O5) is 1.4°, indicating these two groups are almost coplanar. The dihedral angles between two carboxylate groups (O1—C11—O2, O6—C12—O7) and center naphthalene rings are 116.7° and 109.9°, respectively. The dihedral angle between two carboxylate groups (O1—C11—O2, O6—C12—O7) is 22.17°. If we consider two coordination models μ_3-η^1:η^2 and μ_2-η^2:η^1 as μ_1-η^1:η^0 and μ_1-η^1:η^1 temporarily, dna^{2-} acts as a μ_3-bridge to link three different Ba(Ⅱ) ions, which takes as three connection node, resulting in a 2D (6, 3) topology (Fig. 2a). Furthermore, the 2D layers are connected by μ_3-η^1:η^2 and μ_2-η^2:η^1 carboxylate groups to give rise to 3D network structure as shown in Fig. 2b

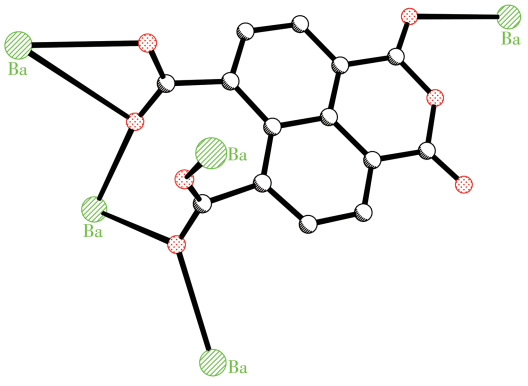

Scheme 1 ORTEP view of coordination model of dna^{2-}

Table 2 Selected bond lengths (nm) and angles (°) for 1

Ba1—O1	0.282 21(17)	Ba1—O7	0.282 63(17)	Ba1—O6	0.277 60(17)
Ba1—O8	0.277 7(2)	Ba1—O2#1	0.261 98(17)	Ba1—O9	0.276 9(2)
Ba1—O3	0.293 11(19)	Ba1—O7#2	0.302 14(19)	Ba1—O2	0.323 07(18)
O2#1—Ba1—O9	93.72(7)	O2#1—Ba1—O6	134.20(5)	O9—Ba1—O6	128.94(6)
O2#1—Ba1—O8	70.04(6)	O9—Ba1—O8	122.37(7)	O6—Ba1—O8	72.61(6)
O2#1—Ba1—O1	115.36(5)	O9—Ba1—O1	66.34(6)	O6—Ba1—O1	75.86(5)
O8—Ba1—O1	72.05(6)	O2#1—Ba1—O7	133.24(5)	O9—Ba1—O7	81.78(7)
O6—Ba1—O7	76.30(5)	O8—Ba1—O7	148.49(6)	O1—Ba1—O7	105.27(5)
O2#1—Ba1—O3	78.67(6)	O9—Ba1—O3	137.44(7)	O6—Ba1—O3	78.83(6)
O8—Ba1—O3	94.52(6)	O1—Ba1—O3	153.93(6)	O7—Ba1—O3	74.34(5)
O2#1—Ba1—O7#2	65.03(5)	O9—Ba1—O7#2	66.92(6)	O6—Ba1—O7#2	140.52(5)
O8—Ba1—O7#2	134.74(5)	O1—Ba1—O7#2	133.16(5)	O7—Ba1—O7#2	70.60(6)
O3—Ba1—O7#2	72.07(5)	O2—Ba1—O2#1	73.47(5)	O9—Ba1—O2	62.37(6)
O6—Ba1—O2	108.96(5)	O8—Ba1—O2	60.00(6)	O1—Ba1—O2	42.27(5)
O7—Ba1—O2	138.14(5)	O7#2—Ba1—O2	109.99(5)	O3—Ba1—O2	147.22(5)

Symmetry codes: #1: 1−*x*, −*y*, 1−*z*; #2: 1−*x*, −1−*y*, 1−*z*.

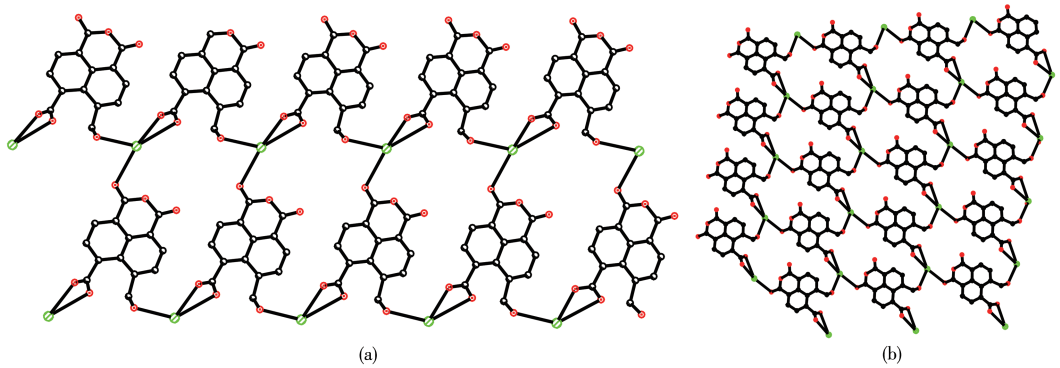

Fig.2 Infinite 2D structure in complex **1**

and Fig.3. In the MOF lattice, the chromophoric naphthalene moieties are separated by a distance of 0.35 nm showing a strong π-π stacking interaction[28].

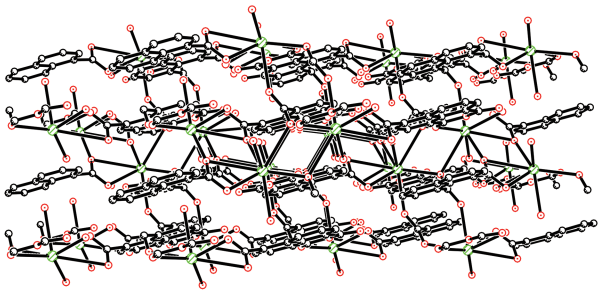

Fig.3 Crystal packing diagram for **1**

2.2 IR spectra of complex 1 and ligand nta

As shown in the ligand nta structure, the anhydride group doesn't exist. This anhydride group was generated from nta after solvothermal reaction with $BaCO_3$. We proposed a possible reaction mechanism as outlined in Scheme 2[29]. In the spectrum of complex **1**, two characteristic absorption bands at 1 776 and 1 706 cm^{-1} are ascribed to the anhydride group of dta^{2-} (Fig.4). The absence of strong bands at 1 700 cm^{-1} indicates the deprotonation of the ligand, which is in accordance with the structural analysis results of **1**. The spectrum exhibited strong broad bands at 1 610 and 1 590 cm^{-1}, which are attributed to asymmetric COO stretching mode, while the peaks at 1 440 and 1 398 cm^{-1} are corresponding to symmetric COO stretching vibration[30]. The differences between the asymmetric and symmetric stretching of the carboxylate groups of

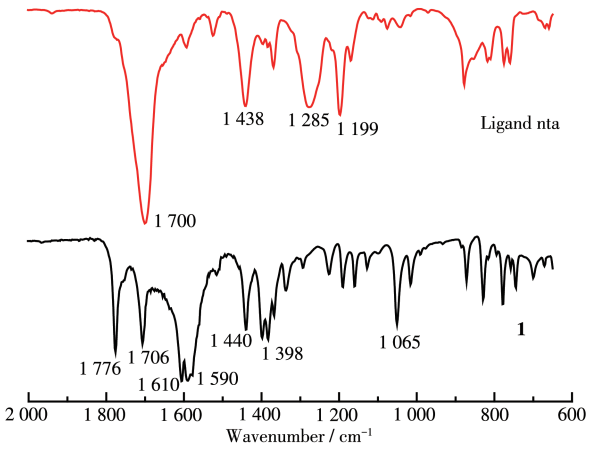

Fig.4 FT-IR spectra of ligand nta and complex **1**

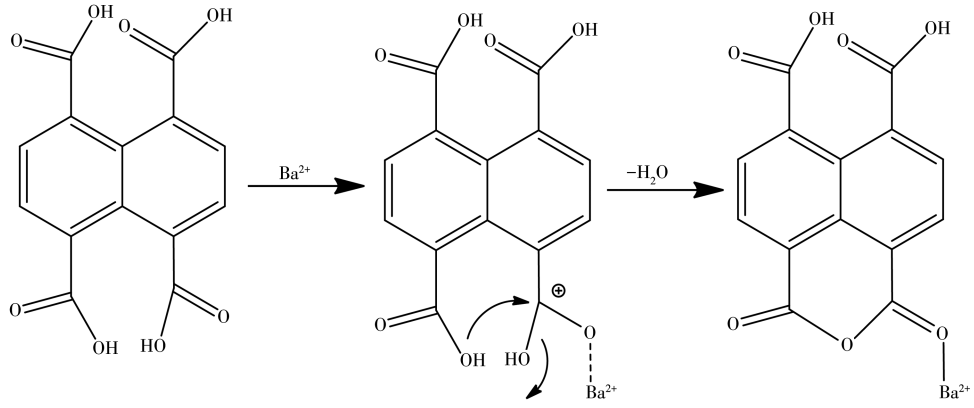

Scheme 2 Forming pathway of 1,8-naphthalic anhydride-4,5-dicarboxylic

1, Δ=192 and 207 cm^{-1}, respectively, suggest a monodentate coordinating between the carboxylate group and barium ion[30]. The difference between the asymmetric and symmetric stretching of the carboxylate groups of **1**, Δ=150 cm^{-1}, indicates the presence of chelating —COO groups[31]. Carboxylic acid anhydrides displayed symmetric and asymmetric carbonyl $(C{=}O)_2$ stretching vibration, respectively. For conjugation carboxylic acid anhydrides, the stronger absorption band of symmetric $(C{=}O)_2$ ranged from 1 770 to 1 780 cm^{-1}, while the weaker absorption band of asymmetric $(C{=}O)_2$ ranged from 1 715 to 1 725 cm^{-1} [31].

2.3 Luminescence properties of complex 1

MOFs have been reported to have the ability to adjust the emission wavelength of organic ligands through the incorporation of metal centers. Therefore, it is important to investigate the luminescence properties of MOFs given potential applications as light-emitting diodes (LEDs) [32]. The luminescent behaviors of the ligand nta and complex **1** were investigated at room temperature using the same weight of powder in the solid-state, and the emission spectra are indicated in Fig. 5. Complex **1** exhibited photoluminescence with maximal emission at 520 nm upon excitation at 320 nm, which was about 100 nm red-shifting compared to ligand nta (maximal emission at 420 nm upon excitation at 290 nm). The observed emissions of complex **1** are probably contributed by the π-π* intra-ligand fluorescence since similar emissions were also observed for the ligand itself[33]. Nevertheless, the large red-shift of maximal emission is considerately attributed to the coordination or an excited state of a metal perturbing intra-ligand. The observed stronger emission intensity of **1** than free ligand implies the increased rigidity of the aromatic backbone of the ligand. This is also attributed to a strong π-π stacking resulting from the enhanced intra-/intermolecular interactions among the organic ligands due to the formation of MOFs, which can facilitate energy transfer[33]. This is well known as aggregation-induced emission (AIE), which is caused by the coordination of organic ligands to metal ions that restricts the deformation of the ligand and induces non-radiative relaxation[34-35].

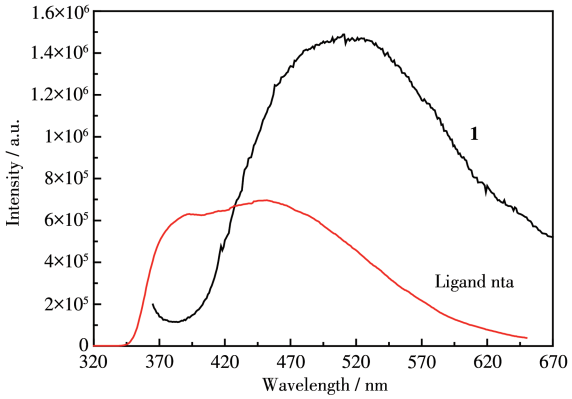

λ_{ex}=320 nm (**1**), 290 nm (nta)

Fig.5 Emission spectra of complex **1** and ligand nta in the solid-state at room temperature

2.4 Detection of aromatic amines

First, the UV-Vis spectra of complex **1** before and after the addition of aromatic amine are given in Fig.6A and 6B. As shown in Fig.6A, with the addition of 1-aminopyrene, the absorbance of the samples in a range of 200 to 400 nm increased gradually. As shown in Fig. 6B, 1-aminopyrene itself had two maximal absorption peaks at 285 and 360 nm, and complex **1** had the maximum at 350 nm, which confirms the absorbance change of 1-aminopyrene after **1** reacted with 1-aminopyrene. Through analysis of the relationship between the absorbance at 350 nm and the added amount, the calculated regression equation and correlation coefficient were y=0.089 29+0.004 01x and 0.989 04, which shows that the enhancement of absorption peak is linearly related to the increase amount of 1-aminopyrene. The changes of the fluorescence intensity of **1** and **1** reacted with different amines are clearly shown in Fig.6C, where it could be found that the highest enhancement was up to 1.7-fold with maximum emission at 445 nm (excited at 320 nm) and the detection limit of 1-aminopyrene was calculated to be down to 0.01 $mg\cdot g^{-1}$ (the ratio of 1-aminopyrene to complex **1**). To explore the specificity of amines detection by complex **1**, aniline and 1-naphthylamine in the same ratios (0.01 $mg\cdot g^{-1}$) were also tested. However, the intensity of their maximum emission increased less than that of **1** with 1-aminopyrene. The photographs of the samples with and without these amines under daylight were also recorded using a digital camera. The

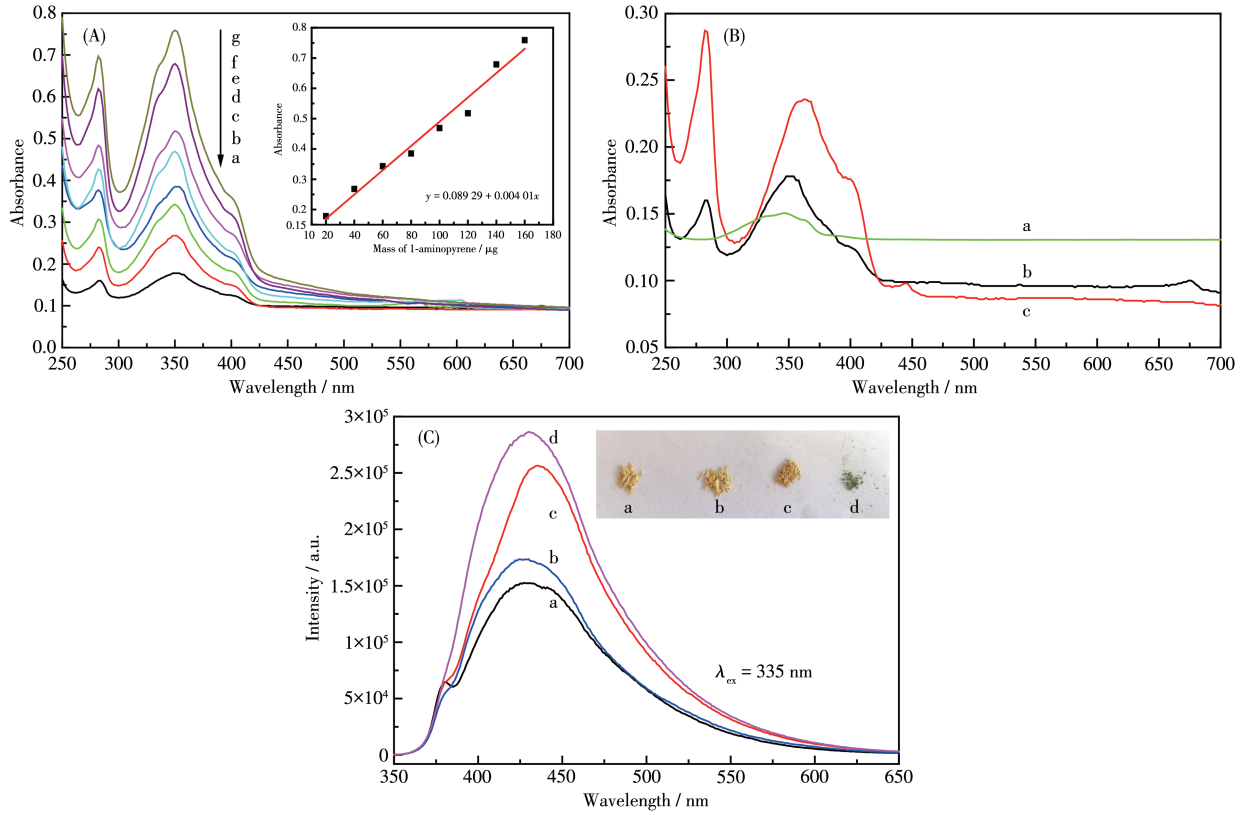

Inset in (A): plot of absorbance at 350 nm vs mass of 1-aminopyrene; Inset in (C): photos of the powder samples

Fig.6　(A) UV-Vis spectra of complex **1** (1 mg) reacted with 1-aminopyrene of different masses ranging from 20 to 160 μg (a-g, respectively); (B) UV-Vis spectra of the samples: (a) **1**, (b) **1** reacted with 20 μg 1-aminopyrene, (c) 1-aminopyrene; (C) Emission spectra of complex **1** before and after reacted with various aromatic amines of 10 μg: (a) **1**, (b) **1** reacted with aniline, (c) **1** reacted with 1-naphthylamine, (d) **1** reacted with 1-aminopyrene

sample of **1** with 1-aminopyrene showed a visible color change from light brown to dark green. These results demonstrated that complex **1** exhibited an optimal enhanced fluorescent response to a low concentration of 1-aminopyrene. Furthermore, the FT-IR spectra (Fig.7) exhibited strong broadband at 1 560 cm^{-1} owing to O═C—N_{as} stretching mode. This further confirms the absorbance change of 1-aminopyrene is mainly related to the reaction of an amino group from aromatic amine and anhydride group from dta^{2-}[36].

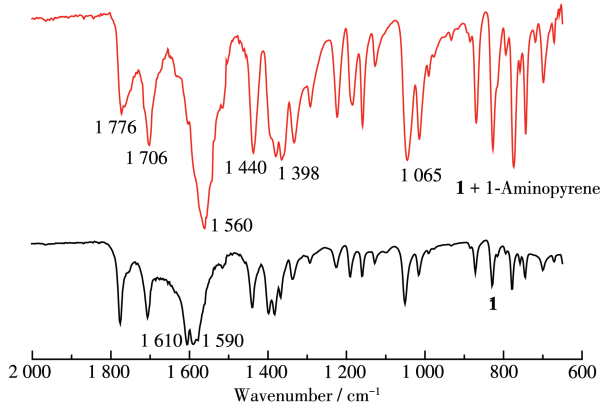

Fig.7　FT-IR spectra of complex **1** and **1** reacted with 1-aminopyrene at 50 ℃

2.5　Thermal stability and precursor for crystalline nano-$BaCO_3$

TGA was used to examine the thermal stability of complex **1**. The TG curve of **1** (Fig. 8) exhibited two main weight loss stages in a temperature ranges of 18-187 ℃ (8.93%) and 307-554 ℃ (35.08%). This first and second weight loss are corresponding to the release of two coordinated water molecules (Calcd. 7.87%) and C_8H_{10} (Calcd. 34.14%, caused by decomposition of the ligand), respectively. The final residue may be $BaCO_3$.

In addition, dehydration and rehydration experiments were performed for **1**, and PXRD was used to determine the phase reversibility. Complex **1** was heated at 300 ℃ for 10 min, to obtain complete loss of

water. The powdered dehydrated phase had a PXRD pattern different from complex **1** (Fig. 9), which indicates that the framework probably shrank after the removal of water. The dehydrated phase was afterward exposed to water vapor at room temperature for another 24 h rehydration. The PXRD pattern of rehydrated sample was similar to that of **1** (see Fig.9), which shows that the dehydration/rehydration process for **1** is reversible.

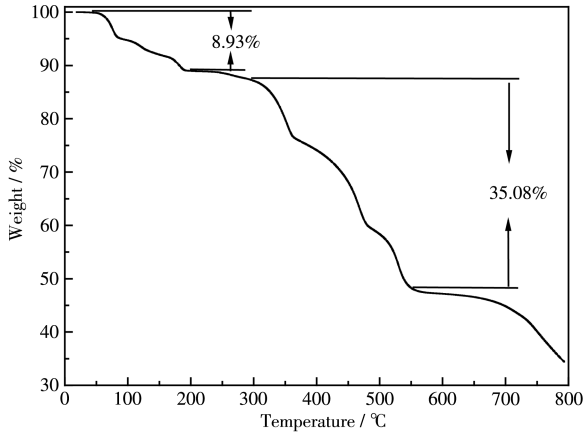

Fig.8 TG curve of **1**

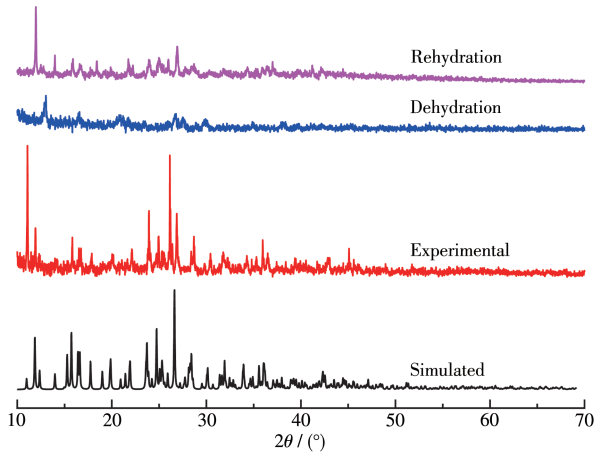

Fig.9 PXRD patterns of simulation of **1** from single-crystal X-ray data and powder samples prepared by dehydration and rehydration process

The morphology of nano-sized $BaCO_3$ powder was studied by scanning electron microscopy (SEM) as shown in Fig.10. SEM images of the particles obtained from the calcination of **1** in the air under different temperatures showed a size range of 0.1-0.41 μm. The PXRD patterns (Fig. 11) confirmed that single-crystalline $BaCO_3$ was formed by the thermal decomposition of **1** at different temperatures (a: 600 ℃, b: 650 ℃, c: 700 ℃) because all the d values (d is the distance between the lattice planes in the crystal) correspond to the reported values with no detectable peaks from impurity[37]. The samples consist of a single phase of well-crystalline $BaCO_3$ with an orthorhombic structure (PDF No. 45-1471) and with lattice parameters of a= 0.643 3 nm, b=0.531 5 nm, c=0.890 4 nm. The strong and sharp diffraction peaks suggest that the prepared $BaCO_3$ is highly crystalline.

To further confirm the polymorphs of as-prepared products at different temperatures, they were characterized by FT-IR spectroscopy and the corresponding results are shown in Fig.12. In general, isolated, planar CO_3^{2-} anion has a D_{3h} symmetry. The absorption bands attributed to the vibrations in CO_3^{2-} anion were located in the 2 000-400 cm^{-1} region. The vibrational spectra of carbonate minerals contain four normal modes: symmetric stretching (ν_1), out-of-plane bending (ν_2), antisymmetric stretching (ν_3), and in-plane bending (ν_4). The strong broad absorption centered at about 1 454 cm^{-1} is ascribed to the asymmetric stretching vibration and two strong sharp absorption bands at about 856 and 694 cm^{-1} can be assigned to out-of-plane bending vibrations and in-plane vibrations, respectively. The result agrees with the XRD analysis and further confirms the formation of $BaCO_3$[38].

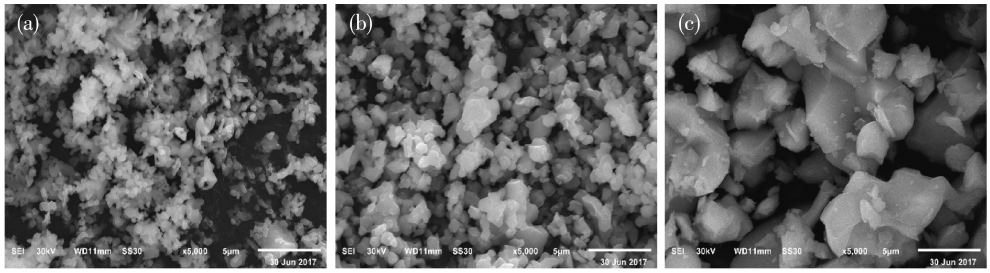

Fig.10 SEM images of $BaCO_3$ obtained by thermolysis of **1** in the air at different temperatures: (a) 600 ℃, (b) 650 ℃, (c) 700 ℃

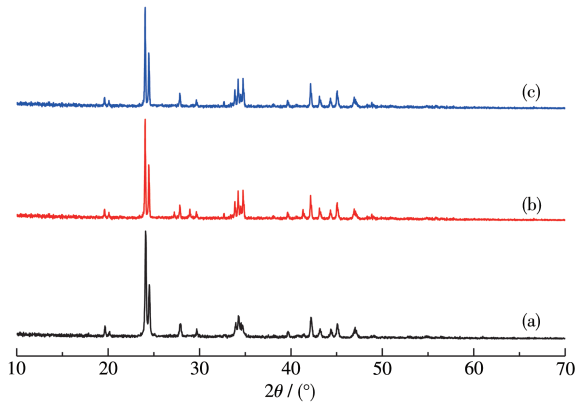

Fig.11 PXRD patterns of $BaCO_3$ obtained by thermolysis of **1** in the air at different temperatures: (a) 600 ℃, (b) 650 ℃, (c) 700 ℃

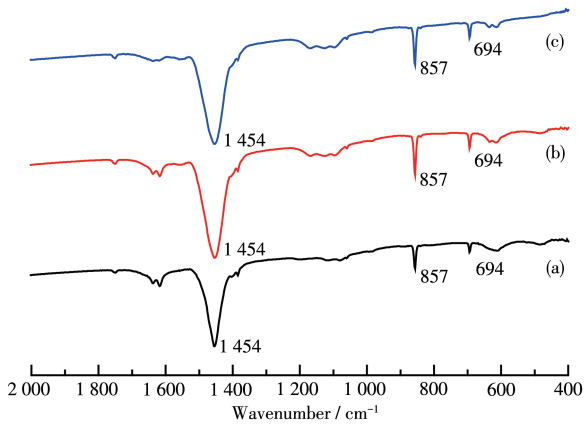

Fig.12 FT-IR spectra of as-synthesized $BaCO_3$ at different temperatures: (a) 600 ℃, (b) 650 ℃, (c) 700 ℃

3 Conclusions

In summary, a new alkaline earth metal barium-complex was synthesized and characterized. In complex **1**, the central Ba^{2+} ion is nine-coordinate with a distorted mono-capped square geometry. Three carboxyl groups take three different coordination modes: μ^1-η^1:η^0, μ^1-η^1:η^1, μ^3-η^2:η^2. The whole dna^{2-} anion acts as a μ_3-bridge connecting three different Ba(Ⅱ) ions resulting in a 3D structure. The fluorescent and thermal stable properties of complex **1** were also investigated. In addition, it offers a "turn-on" sensing behavior for aromatic amines with a low detection limit. This polymer precursor was also thermally decomposed to prepare micro-crystal calcite particles.

Acknowledgments: This work is supported by the National Natural Science Foundation of China (Grant No. 21671107), Science Research Starting Project of Chuzhou University (Grant No. 2014qd035), Foundation of Nanjing Xiaozhuang University (Grant No. 2017NXY11), College Student Innovation and Entrepreneurship Training Program (Grants No. 202011460070Y, 2020XSKY089).

References:

[1]Merchant Z M, Cheng S G G. Developments in Characterization of Foods Using Antibodies//Gaonkar A G. *Characterization of Foods, Emerging Methods*. New York: Elsevier Science, **1995**:347-376

[2]Bao B, Yuwen L L, Zheng X, Weng L, Zhu X, Zhan X, Wang L. A Fluorescent Conjugated Polymer for Trace Detection of Diamines and Biogenic Polyamines. *J. Mater. Chem.*, **2010**,**20**(43):9628-9634

[3]Kaur N, Chopra S, Singh G, Raj P, Bhasin A, Sahoo S K, Kuwar A, Singh N. Chemosensors for Biogenic Amines and Biothiols. *J. Mater. Chem. B*, **2018**,**6**(30):4872-4902

[4]Medina M Á, Urdiales J L, Rodríguez-Caso C, Ramírez F J, Sanchez-Jiménez F. Biogenic Amines and Polyamines: Similar Biochemistry for Different Physiological Missions and Biomedical Applications. *Crit. Rev. Biochem. Mol. Biol.*, **2003**,**38**(1):23-59

[5]Kumpf J, Bunz U H F. Aldehyde-Appended Distyrylbenzenes: Amine Recognition in Water. *Chem. Eur. J.*, **2012**,**18**(29):8921-8924

[6]Comes M, Marcos M D, Martinez-Manez R, Sancenon F, Soto J, Villaescusa L A, Amoros P, Beltran D. Chromogenic Discrimination of Primary Aliphatic Amines in Water with Functionalized Mesoporous Silica. *Adv. Mater.*, **2004**,**16**(20):1783-1786

[7]Hinoue T, Miyata M, Hisaki I, Tohnai N. Guest-Responsive Fluorescence of Inclusion Crystals with π-Stacked Supramolecular Beads. *Angew. Chem. Int. Ed.*, **2012**,**51**(1):155-158

[8]Stetter J R, Penrose W R, Yao S. Sensors, Chemical Sensors, Electrochemical Sensors, and ECS. *J. Electrochem. Soc.*, **2003**,**150**(2):11-16

[9]Zhou D Y, Wang Y Y, Jia J, Yu W Z, Qu B F, Li X, Sun X. H-Bonding and Charging Mediated Aggregation and Emission for Fluorescence Turn-On Detection of Hydrazine Hydrate. *Chem. Commun.*, **2015**,**51**(53):10656-10659

[10]Mani P, Ojha A A, Reddy V S, Mandal S. "Turn-On" Fluorescence Sensing and Discriminative Detection of Aliphatic Amines Using a 5-Fold-Interpenetrated Coordination Polymer. *Inorg. Chem.*, **2017**,**56**(12):6772-6775

[11]Yin X M, Gao L L, Li P, Bu R, Sun W J, Gao E Q. Fluorescence Turn-On Response Amplified by Space Confinement in Metal-Organic Frameworks. *ACS Appl. Mater. Interfaces*, **2019**,**11**(50):47112-47120

[12]刘志强, 黄永清, 孙为银. 金属有机框架化合物对溶剂分子和有机小分子荧光识别与传感研究进展. 无机化学学报, **2017**,**33**(11):1959-1969

Liu Z Q, HUANG Y Q, SUN W Y. Progress in Fluorescent Recognition and Sensing of Solvent and Small Organic Molecules Based on Metal-Organic Frameworks. *Chinese J. Inorg. Chem.*, **2017**,**33**(11):1959-1969

[13]刘珍, 陈晓, 冯云龙. 基于一个四羧酸配体构筑的具有(4,8)-连接的镧系金属有机框架材料及对小分子的检测试验. 无机化学学报, **2016**,**32**(8):1413-1420
LIU Z, CHEN X, FENG Y L. Two Series of (4,8)-Connected Lanthanide-Metal Organic Frameworks Based on a Tetra-carboxylate Ligand for Sensing of Small Molecules. *Chinese J. Inorg. Chem.*, **2016**, **32**(8):1413-1420

[14]Kreno L E, Leong L E, Farha O K, Allendorf M, Van Duyne R P, Hupp J T. Metal-Organic Framework Materials as Chemical Sensors. *Chem. Rev.*, **2012**,**112**(2):1105-1125

[15]Yu C X, Chen J, Zhang Y, Song W B, Li X Q, Chen F J, Zhang Y J, Liu D, Liu L L. Highly Efficient and Selective Removal of Anionic Dyes from Aqueous Solution by Using a Protonated Metal-Organic Framework. *J. Alloys Compd.*, **2021**,**853**:157383

[16]Mallick A, El-Zohry A M, Shekhah O, Yin J, Jia J T, Aggarwal H, Emwas A, Mohammed O F, Eddaoudi M. Unprecedented Ultralow Detection Limit of Amines Using a Thiadiazole-Functionalized Zr(Ⅳ)-Based Metal-Organic Framework. *J. Am. Chem. Soc.*, **2019**,**141**(18): 7245-7249

[17]Hazra A, Bej S, Mondal A, Murmu N C, Banerjee P. Discerning Detection of Mutagenic Biopollutant TNP from Water and Soil Samples with Transition Metal-Containing Luminescence Metal-Organic Frameworks. *ACS Omega*, **2020**,**5**(26):15949-15961

[18]Deng H X, Grunder S, Cordova K E, Valente C, Furukawa H, Hmadeh M, Gandara F, Whalley A C, Liu Z, Asahina S, Kazumori H, O'Keeffe M, Terasaki O, Stoddart J F, Yaghi O M. Large-Pore Apertures in a Series of Metal-Organic Frameworks. *Science*, **2012**, **336**(6084):1018-1023

[19]Van-Humbeck J F, McDonald T M, Jing X, Wiers B M, Zhu G, Long J R. Ammonia Capture in Porous Organic Polymers Densely Functionalized with Brønsted Acid Groups. *J. Am. Chem. Soc.*, **2014**,**136** (6):2432-2440

[20]Marsh C, Han X, Li J N, Lu Z Z, Argent S P, Silva I, Cheng Y Q, Daemen L L, Ramirez-Cuesta A J, Thompson S P, Blake A J, Yang S H, Schröder M. Exceptional Packing Density of Ammonia in a Dual-Functionalized Metal-Organic Framework. *J. Am. Chem. Soc.*, **2021**, **143**(17):6586-6592

[21]Sun L B, Li Y, Liang Z Q, Yua J H, Xua R R. Structures and Properties of Lanthanide Metal-Organic Frameworks Based on a 1,2,3-Triazole-Containing Tetracarboxylate Ligand. *Dalton Trans.*, **2012**, **41**:12790-12796

[22]Fan L M, Fan W L, Li B, Liu X Z, Zhao X, Zhang X T. Structural Diversities and Related Properties of Four Coordination Polymers Synthesized from Original Ligand of 3,3′,5,5′-Azobenzenetetracarboxylic Acid. *Dalton Trans.*, **2015**,**44**:2380-2389

[23]Cui Y J, Yue Y F, Qian G D, Chen B L. Luminescent Functional Metal-Organic Frameworks. *Chem. Rev.*, **2012**,**112**(2):1126-1162

[24]Wu G, Feng J H, Wang X F. Synthesis, Crystal Structure, and Physical Properties of a Barium(Ⅱ) Benzene-1,2,3-tricarboxylic Acid Complex. *Z. Anorg. Allg. Chem.*, **2012**,**638**(6):1047-1052

[25]Wang X F, Yu L, Wei H, Wu G. Synthesis, Crystal Structure, and Physical Properties of a Barium(Ⅱ) *p*-(Carboxy-l-methyloxy)-benzenecarboxylic Acid Complex. *Z. Anorg. Allg. Chem.*, **2011**,**637**(2):289-292

[26]Al-Terkawi A, Scholz G, Emmerling F, Kemnitz E. Barium Coordination Polymers Based on Fluorinated and Fluorine-Free Benzene-Dicarboxylates: Mechanochemical Synthesis and Spectroscopic Characterization. *Solid State Sci.*, **2018**,**79**:99-108

[27]Wu G, Zhang S Q, Guo L. Synthesis, Structure, and Properties of a New Calcium(Ⅱ) Complex of 1,10-Phenanthroline, 1,2,4,5-Benzenetetracarboxylic Acid, and a New Precursor to Produce Pure Phase Microcrystalline Calcite Particles. *Z. Anorg. Allg. Chem.*, **2013**,**639** (5):804-809

[28]Thakuria R, Nath N K, Saha B K. The Nature and Applications of π-π Interactions: A Perspective. *Cryst. Growth Des.*, **2019**,**19**(2):523-528

[29]Xu T, Mohr S, Amende M, Laurin M, Döpper T, Görling A, Libuda J. Benzoic Acid and Phthalic Acid on Atomically Well-Defined MgO (100) Thin Films: Adsorption, Interface Reaction, and Thin Film Growth. *J. Phys. Chem. C*, **2015**,**119**(48):26968-26979

[30]Nyquist R A. *Interpreting Infrared, Raman, and Nuclear Magnetic Resonance Spectra*: *Vol*. 1. *Elsevier*, **2001**:205

[31]Nakamoto K. *Infrared and Raman Spectra of Inorganic and Coordination Compounds, Part B, Applications in Coordination, Organometallic, and Bioinorganic Chemistry*. *5th ed. Wiley*, **1997**:59-62

[32]Li Y L, Zhao Y, Wang P, Kang Y S, Liu Q, Zhang X D, Sun W Y. Multifunctional Metal-Organic Frameworks with Fluorescent Sensing and Selective Adsorption Properties. *Inorg. Chem.*, **2016**,**55**(22): 11821-11830

[33]Zheng X F, Zhou L, Huang Y M, Wang C G, Duan J G, Wen L L, Tian Z F, Li D F. A Series of Metal-Organic Frameworks Based on 5-(4-Pyridyl)-isophthalic Acid: Selective Sorption and Fluorescence Sensing. *J. Mater. Chem. A*, **2014**,**2**(31):12413-12422

[34]Xu Y, Tao C L, Yu M X, Xiong Y, Ouyang Y N, Liu X G, Zhao Z J. Tetraphenylethene-Based Luminescent Metal-Organic Framework for Effective Differentiation of *cis*/*trans* Isomers. *ACS Appl. Mater. Interfaces*, **2020**,**12**(31):35266-35272

[35]Liu C Y, Chen X R, Chen H X, Niu Z, Hirao H, Braunstein P, Lang J P. Ultrafast Luminescent Light-Up Guest Detection Based on the Lock of the Host Molecular Vibration. *J. Am. Chem. Soc.*, **2020**,**142** (14):6690-6697

[36]Zhang H Y, Nie Y Z, Zhi X M, Du H F, Yang J. Controlled Ring-Opening Polymerization of α-Amino Acid *N*-Carboxy-anhydride by Frustrated Amine/Borane Lewis Pairs. *Chem. Commun.*, **2017**, **53** (37):5155-5158

[37]Dadkhah M, Salavati-Niasari M, Davar F. A New Inorganic Framework in the Synthesis of Barium Carbonate Nanoparticles via Convenient Solid State Decomposition Route. *Adv. Powder Technol.*, **2013**, **24**(1):14-20

[38]Tabatabaee M, Kukovec B M, Amjad S, Shishebor M R. Two Different Barium(Ⅱ) 2D Coordination Polymers Constructed with Pyrazine-2, 3-dicarboxylate: Synthesis, Crystal Structures, and Thermal Decomposition to Barium (Ⅱ) Carbonate Nanoparticles. *Aust. J. Chem.*, **2016**,**69**(11):1261-1267